

RSC Advances



This article can be cited before page numbers have been issued, to do this please use: Z. Dai, X. Yu, C. Huang, M. Li, J. Su, Y. Guo, H. Xu and Q. Ke, *RSC Adv.*, 2016, DOI: 10.1039/C6RA15463H.



This is an *Accepted Manuscript*, which has been through the Royal Society of Chemistry peer review process and has been accepted for publication.

Accepted Manuscripts are published online shortly after acceptance, before technical editing, formatting and proof reading. Using this free service, authors can make their results available to the community, in citable form, before we publish the edited article. This *Accepted Manuscript* will be replaced by the edited, formatted and paginated article as soon as this is available.

You can find more information about *Accepted Manuscripts* in the [Information for Authors](#).

Please note that technical editing may introduce minor changes to the text and/or graphics, which may alter content. The journal's standard [Terms & Conditions](#) and the [Ethical guidelines](#) still apply. In no event shall the Royal Society of Chemistry be held responsible for any errors or omissions in this *Accepted Manuscript* or any consequences arising from the use of any information it contains.

Nanocrystalline MnO₂ on Activated Carbon Fiber for Catalytic Formaldehyde Removal

Received 00th January 20xx,
Accepted 00th January 20xx

DOI: 10.1039/x0xx00000x

www.rsc.org/

Zijian Dai^a, Xiaowei Yu^b, Chen Huang^a, Meng Li^a, Jiafei Su^b, Yaping Guo^b, He Xu^b, Qinfei Ke,^{*,b,a}

Three different types of nanocrystalline MnO₂ namely α -MnO₂, γ -MnO₂ and δ -MnO₂ were successfully synthesized by the co-precipitated method, which has the advantages of easy preparation, low cost, size uniformity and excellent crystalline. It also avoids operating at high temperatures and pressures. The nanocrystalline MnO₂ were then tested for formaldehyde catalytic oxidation at 25 °C. The results suggested that δ -MnO₂ had the highest catalytic activity. Hence, δ -MnO₂ was synthesized by the same method to modify the activated carbon fiber (ACF) substrate. Further tests showed that the as-prepared MnO₂/ACF samples could significantly improve the removal of formaldehyde at room temperature. MnO₂ contents in MnO₂/ACF had a great influence on the breakthrough time and we found that the MnO₂ contents were not better at greater magnitudes but rather optimal at 16.12 wt%. The formation method developed in this study might become a promising technique to improve the catalytic activity in formaldehyde removal.

Introduction

Among various volatile organic compounds (VOCs), formaldehyde remains to be a major pollutant, especially in indoor environment. Formaldehyde is emitted from construction and decoration materials, and can cause physical and mental illness at elevated concentrations (WHO 2006). What is worse, exposure to the formaldehyde environment would result in nasopharyngeal cancer and other serious diseases in humans.¹⁻³ Thus, the removal of formaldehyde in indoor environment is of utmost importance.

A lot of methods have been used for formaldehyde removal, among which physical adsorption,^{2, 4} catalytic oxidation^{5, 6} and plasma decomposition^{7, 8} are most commonly used. However, these methods have certain limitations. For physical adsorption approach which is most widely used in commercial air-cleaner, short saturated absorption time and difficult treatment of abandoned adsorbent make it less effective. For catalytic oxidation approach,

many chemical catalysts only work in severe condition, e.g., TiO₂ becomes less effective without UV light and may generate harmful byproducts during the catalytic processes,⁹ most of the metal catalysts have to work at high temperature, and the exorbitant prices of noble metal catalysts made it impractical to be popularized.¹⁰⁻¹² Plasma technology showed poor performance under low concentrations and is also easy to generate harmful byproducts.³ Based on these studies, the combination of adsorption and catalytic oxidation should be an improved method to remove indoor formaldehyde at low concentration.¹³

Activated carbon fiber (ACF) has been regarded as the most promising adsorbent in formaldehyde removal due to the abundant micro pores, large surface area, low pressure drop and excellent adsorption capacity.^{4, 14, 15} The adsorption capacity of ACF for formaldehyde is not ideal in ambient temperature, because of the weak interaction between polar formaldehyde and the hydrophobic surface of porous carbon.^{16, 17} In order to enhance the adsorption capacity of ACF, some studies utilized surface modification to promote the adsorption property, e.g., introducing a functional substance such as p-aminobenzoic acid,¹⁷ CuO¹⁸ and TiO₂.¹⁹ Other transition metal oxide catalysts have also been proved to possess high catalytic activity for HCHO complete oxidation, such as CeO₂,^{11, 20-22} Co₃O₄²³⁻²⁵ and MnO₂.^{13, 26-28} While most of the previous research focused on the removal of high-concentration

^a Key Laboratory of Textile Science & Technology (College of Textiles, Donghua University), Ministry of Education, Shanghai 201620, P. R. China. E-mail: kqf@dhu.edu.cn

^b Environmental Materials Research Center, Shanghai Normal University, Shanghai 200234, P. R. China

† Footnotes relating to the title and/or authors should appear here.

Electronic Supplementary Information (ESI) available: [Summary of the catalytic oxidation for formaldehyde removal at ambient temperature in recent literature in Table S1 and amounts of δ -MnO₂ attached in MnO₂/ACF in Table S2. The formaldehyde removal amount was calculated.] See DOI: 10.1039/x0xx00000x

formaldehyde (>100 ppm), in indoor environment, however, the concentration of formaldehyde is generally low. Therefore, the investigation in catalyst capacities of the formaldehyde at low concentration levels has practical implications.

Recently, a multitude of researches have concerned formaldehyde catalytic removal at ambient temperature.^{6, 13, 27, 29-35} Table S1 summarized the reported catalytic materials, concentration level, temperature, test methods, and their activities on the catalytic oxidation of formaldehyde at ambient temperature over related catalysts. To our knowledge, no research has focused on formaldehyde removal using MnO₂-based ACF substrates.

Herein, three kinds of nanocrystalline MnO₂ with different phase structures (α -MnO₂, γ -MnO₂ and δ -MnO₂) were synthesized by the co-precipitated method. MnO₂ was selected because no harmful byproducts were generated during the formaldehyde oxidation process.³⁶ Catalytic tests at room temperature revealed that δ -MnO₂ had the best activity. Based on this result, ACF were modified with δ -MnO₂, and the obtained samples showed significant removal of formaldehyde.

Experimental

Materials. KMnO₄, MnSO₄ (analytical pure reagent) were purchased from Sinopharm Chemical Reagent Co., Ltd and used without further purification. The Pitch-based ACF was obtained from Osaka Gas Chemicals Co., Ltd. ACF was first washed with deionized water for three times to remove ash and dried at 130 °C for 12 h in vacuum before use.

Synthesis of α -MnO₂, γ -MnO₂ and δ -MnO₂. The α -MnO₂, γ -MnO₂ and δ -MnO₂ were prepared by a co-precipitation method. The redox reaction was listed as follows:^{37, 38}



To synthesize α -MnO₂, 3.16 g KMnO₄ and 4.53 g MnSO₄ were dissolved in 50 mL deionized water respectively and kept stirring at 90 °C. Then the KMnO₄ and MnSO₄ solution were added dropwise into 50 mL deionized water, respectively. The obtained solution was then kept stirring and reacted at 90 °C for 2 h. The products were washed, centrifuged, and dried at 80 °C for 12 h. For γ -MnO₂, 3.16 g KMnO₄ and 18.12 g MnSO₄ were synthesized at 80 °C for 2 h. For δ -MnO₂, 3.16 g KMnO₄ and 2.26 g MnSO₄ were synthesized at 80 °C for 2 h.

Preparation of δ -MnO₂ Modified ACF. Nanocrystalline MnO₂ were incorporated in ACF by a co-precipitation method. Briefly, ACF was first immersed in MnSO₄ solution, and then KMnO₄ solution was added dropwise and kept stirring violently at 80 °C for 2 h. Subsequently, the ACF was taken out and heated to 80 °C for 12 h, finally dried at 120 °C for 5 h *in vacuum*. By altering the concentration of KMnO₄ and MnSO₄ solution, different MnO₂ content in MnO₂/ACF could be obtained.

Characterization. Scanning electron microscopy (SEM) images were carried out on a Hitachi S-4800 field emission scanning electron microscope. X-ray diffraction (XRD) patterns were measured on a D/max-II B, (SHIMADZU, Japan) using Cu K α radiation ($\lambda = 0.1542$ nm) operated at 40 kV and 30 mA. The α -MnO₂, γ -MnO₂, δ -MnO₂, ACF and MnO₂/ACF were scanned from 5° to 90° with a rate of 5° min⁻¹. The δ -MnO₂ content of each MnO₂/ACF was determined according to ASTM D2866-11. Ash content in individual ACF (n=5) was first measured by following methods. The crucible was placed in a furnace at 650 °C for 1 h, cooled down to room temperature to record the weight (W_0). Next, the ACF was added into the crucible, and its weight was calculated (W_1). Then the crucible was transferred into a preheated muffle furnace at 650 °C for 3 h. Finally, the crucible was cooled to room temperature in a desiccator, and its weight was recorded as W_2 . The ash content was calculated using the Eq (2):

$$\text{Ash}(\%) = \frac{W_2 - W_0}{W_1 - W_0} \times 100 \quad (2)$$

Then the MnO₂/ACF was added into the crucible, total weight was calculated (W_3). The crucible was put into the muffle furnace at a temperature of 650 °C for 3 h. Finally, the crucible was placed in a desiccator for conditioning, and its weight was determined (W_4). The weight of ash in MnO₂/ACF was defined as W_5 . The δ -MnO₂ content of each MnO₂/ACF was derived as follows;

$$W_5 = (W_3 - W_4) \times \text{Ash}\% + (W_3 - W_4) \times \text{Ash}\% \quad (3)$$

$$\delta\text{-MnO}_2(\%) = \frac{W_4 - W_0 - W_5}{W_3 - W_0} \times 100 \quad (4)$$

Nitrogen adsorption-desorption isotherms of ACF and MnO₂/ACF were measured on an ASAP 2020 (Micromeritics Instrument, USA) at 77 K. The surface area of the α -MnO₂, γ -MnO₂, δ -MnO₂, ACF and MnO₂/ACF were obtained based on the Brunauer-Emmett-Teller.^{2, 39} Pore size distributions of α -MnO₂, γ -MnO₂, δ -MnO₂, ACF and MnO₂/ACF were calculated by non-localized density functional theory (NLDFT).⁴⁰ X-ray photoelectron spectroscopy (XPS) was

performed on a PHI5700 ESCA system equipped with aluminum anode (Al K α = 1486.6 eV radiation) at a pressure of 2×10^7 Torr. All the binding energies were calibrated using contaminated carbon (C1s = 284.6 eV). The number of binding energy peaks was determined by the deconvolution process. Hydrogen temperature-programmed reduction (H₂-TPR) measurements were performed with Chemisorption Analyzer (AutoChem II 2920), the H₂ consumption and the mass signal was detected by a thermal conductivity (TCD). δ -MnO₂, ACF and MnO₂/ACF (ca. 50 mg) were introduced in the U-type quartz microreactor with a flow of 5% H₂/Ar at a rate of 50 mL min⁻¹. The samples were heated from 60 °C to 800 °C at a rate of 10 °C min⁻¹.

Adsorption and Catalytic Activity Tests. The room temperature adsorption and catalytic activity measurements of α -MnO₂, γ -MnO₂, δ -MnO₂, ACF and MnO₂/ACF were performed in a fixed-bed quartz reactor (length = 500 mm, diameter = 10 mm) at 25 °C. Gas formaldehyde was generated by flowing pure air (20 \pm 2% RH) through an S-4000 Gas Mixing system (EnviroNics, USA) and the total gas flow rate was 200 mL min⁻¹, monitored by a mass flow control system. The concentration of formaldehyde was kept at 15 ppm. For three different MnO₂, 100 mg samples were used in each test, corresponding to a gas hourly space velocity (GHSV) of 120 000 mL (g_{cat} h)⁻¹. While 200 mg MnO₂/ACF samples with a packing length of 20 mm were kept in quartz reactor in each test, and GHSV was 60 000 mL (g_{cat} h)⁻¹. HCHO, CO₂, CO and water vapor were analyzed online by a photoacoustic IR multigas monitor (INNOVA AirTech Instruments Model 1412i). Before each test, the upstream concentration was first measured for at least 4 h to ensure the HCHO concentration was constant. During the test, the downstream gas was also collected hourly and subsequently analyzed by a GC 9800 gas chromatograph equipped with TCD and FID detectors. No other carbon containing compounds except CO₂ in the products were detected for the tested catalysts. HCHO conversion was determined by the following equation:

$$\text{HCHO conversion (\%)} = \frac{[\text{HCHO}]_{\text{in}} - [\text{HCHO}]_{\text{out}}}{[\text{HCHO}]_{\text{in}}} \times 100 \quad (5)$$

Where [HCHO]_{in} (ppm) is the inlet concentration of HCHO before passing the catalyst, and [HCHO]_{out} (ppm) is the output concentration of HCHO after passing the catalyst. Such above parameters of HCHO conversion were used for calculating the removal capacity of MnO₂/ACF samples.

The activity tests were also performed in static state to clarify the mechanism for HCHO removal. The method of static activity tests was adapted from previous reports.^{29, 31} A stainless steel reactor with a volume of 0.5 L was covered by a polytetrafluoroethylene layer on its inner wall. The MnO₂/ACF sample was first placed on the bottom of a quartz Petri dish. After putting the dish into the reactor, 300 ppm of HCHO was emitted into the reactor using an S-4000 Gas Mixing system (EnviroNics, USA). After the concentration of HCHO was stabilized at 150 ppm, the cover of the sample dish was removed to start the adsorption and catalytic reaction of HCHO. HCHO, CO₂, CO and water vapor were measured respectively during test at 25 °C. The yield of CO₂ (Δ CO₂) and the concentration variation of HCHO were calculated to analyze the removal ratio.

Results and discussion

Morphology Characterization. Fig. 1 depicted the procedure of MnO₂/ACF synthesis. Nanocrystalline MnO₂ were incorporated in ACF by a co-precipitation method. Fig. 2a-f showed the SEM images of α -MnO₂, γ -MnO₂, δ -MnO₂, ACF, 0.03-MnO₂/ACF and 0.05-MnO₂/ACF. The morphology of each MnO₂ sample was determined by different crystal phases. α -MnO₂ showed a needle-like morphology with the diameters of 50 nm and lengths of 300-900 nm. γ -MnO₂ presented an irregular nanoparticle structure, while δ -MnO₂ displayed a flower-like nanostructure without clear interparticle boundaries with an average diameter of 200 nm. As shown in Fig. 2d, the surface of ACF was smooth before loaded with MnO₂. After loading, the surface of ACF became coarser (see Fig. 2e-f). When the concentration of MnSO₄ reached at 0.05 mol L⁻¹, the entire fiber surface was covered by MnO₂, suggesting the maximum MnSO₄ feeding capacity was 0.03 mol L⁻¹.

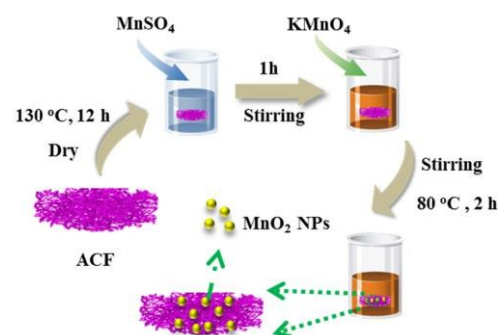


Fig. 1 Scheme of MnO₂/ACF synthesis.

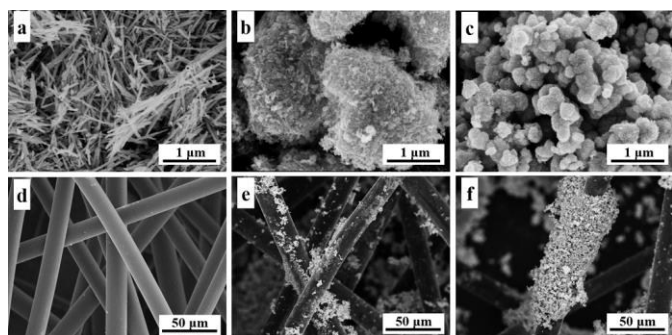


Fig. 2 SEM images of (a) α -MnO₂, (b) γ -MnO₂, (c) δ -MnO₂, (d) ACF, (e) 0.03-MnO₂/ACF and (f) 0.05-MnO₂/ACF.

XRD Analysis. XRD patterns were measured to identify the crystallographic structures of α -MnO₂, γ -MnO₂, δ -MnO₂, ACF and MnO₂/ACF (see Fig. 3).

As shown in Fig. 3, the typical peaks of different MnO₂ can be clearly identified as α -MnO₂ (JCPDS 44-0141), γ -MnO₂ (JCPDS 14-0644) and δ -MnO₂ (JCPDS 80-1098). The ACF pattern obtained two broad diffraction peaks at 25° and 43°, respectively, both of them were characteristics peaks of disordered carbon.^{41,42} Compared to pure ACF pattern, the pattern of MnO₂/ACF showed more diffraction peaks at 12.5°, 37.1° and 66.0°, which were in accordance to the characteristics peaks of δ -MnO₂, suggesting that the δ -MnO₂ has been successfully loaded on the surface of ACF.

Content of δ -MnO₂. The initial ash content in pure ACF sample was ~6.72%. The contents of δ -MnO₂ in MnO₂/ACF samples were calculated by Eq (5) and the result were ~5.62%, 11.74%, 16.12%, 22.42% and 29.33%, depending on the initial concentration of

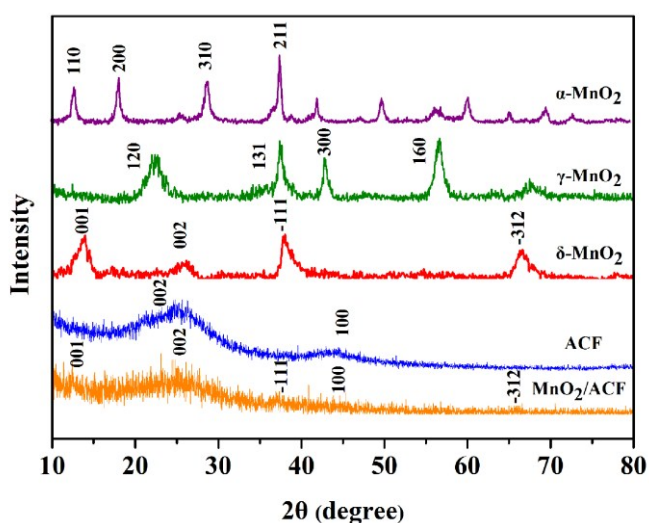


Fig. 3 XRD patterns of α -MnO₂, γ -MnO₂, δ -MnO₂, ACF and MnO₂/ACF.

MnSO₄ solution (0.01 mol L⁻¹, 0.02 mol L⁻¹, 0.03 mol L⁻¹, 0.04 mol L⁻¹, 0.05 mol L⁻¹, respectively). The obtained MnO₂/ACF samples with different δ -MnO₂ contents were labeled as #X MnO₂/ACF (X represented the concentration of MnSO₄ solution). The detailed information was shown in Table S2.

Specific surface area and Porosity. Table 1 lists the specific surface areas (S_{BET}), average pore sizes (D_p) and total pore volumes (V_p) of α -MnO₂, γ -MnO₂ and δ -MnO₂. The δ -MnO₂ exhibited the highest S_{BET} , D_p and V_p values. Nitrogen adsorption isotherms at 77 K of ACF, 0.03-MnO₂/ACF and 0.04-MnO₂/ACF were presented in Fig. 4a. The curve of ACF exhibited type I isotherm, according to the IUPAC classification,⁴³ which indicated that the sample was microporous. With the presence of MnO₂, a hysteresis loop emerged in the adsorption-desorption isotherms, which was attributed to the capillary condensation in mesopores of MnO₂. The relevant BET surface areas of ACF and MnO₂/ACF are shown in Fig. 4a. The results showed that pure ACF had the highest value of 961.20 m² g⁻¹, whereas 0.03-MnO₂/ACF and 0.04-MnO₂/ACF showed the value of 679.12 m² g⁻¹ and 574.92 m² g⁻¹, respectively. The results showed that as more nanocrystalline MnO₂ were loaded on ACF, slight decrease of the surface area was occurred. This is because that nanocrystalline MnO₂ on the surface of ACF blocked the pores, leading the adsorption amount to decrease.⁴² Fig. 4(b) showed the pore size distribution of ACF, 0.03-MnO₂/ACF and 0.04-MnO₂/ACF. Besides the micropores, mesoporous values were also observed in the patterns of 0.03-MnO₂/ACF and 0.04-MnO₂/ACF, which was identical to the results of the adsorption-desorption isotherms. The results also indicated that the pore size increased with the increase of MnO₂ loading amount.

Activity Test. The HCHO oxidation activities of three kinds of MnO₂ catalysts are shown in Fig. 5. The catalytic activities of δ -MnO₂ decreased dramatically at first 5 hours, and the rate of HCHO conversion maintained at ~25% after 40 hours. The other catalysts, α -MnO₂ and γ -MnO₂ showed lower catalytic activities than that of δ -MnO₂. The HCHO conversion using α -MnO₂ turned to 20% after 40 hours. Because the pattern of α -MnO₂ manifested a similar trait to δ -MnO₂, the α -MnO₂ catalyst had an oxidation activity similar with δ -MnO₂. γ -MnO₂ displayed the lowest catalytic activity. A low conversion rate was found at the beginning of the test, after which it dropped continuously and then stabilized at 15%. Previous studies^{28,44} have found that compared with other properties (such

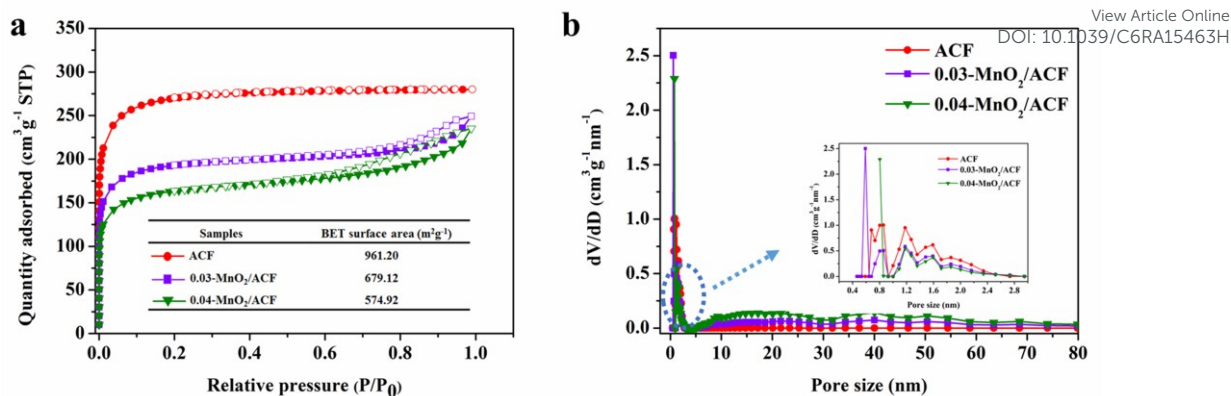


Fig. 4 (a) Nitrogen adsorption/desorption isotherms and (b) corresponding pore size distributions for ACF, 0.03-MnO₂/ACF and 0.04-MnO₂/ACF.

as specific surface area, degree of crystallinity, reducibility and oxidation state of manganese), the tunnel structures of MnO₂ is the primary factor to determine catalytic activity. δ -MnO₂ normally forms a 2D layer structure, while α -MnO₂ and γ -MnO₂ obtained 1D tunnels in their structures. In detail, for α -MnO₂, it consists of [2 × 2] and [1 × 1] channels and γ -MnO₂ contains both [1 × 1] and [1 × 2] channels.⁴⁵ Since the effective diameter of the [2 × 2] channel was more suitable for the HCHO diffusion and adsorption of HCHO molecules than [1 × 1] channel during the reaction, the α -MnO₂ had higher catalytic activity in HCHO oxidation compared with γ -MnO₂. For δ -MnO₂, the interlayer structure would facilitate the diffusion and adsorption of HCHO molecules to active sites more than the [2 × 2] channel, so the δ -MnO₂ showed the best catalytic activity. Therefore, δ -MnO₂ was selected in this article to modify ACF in order to enhance the oxidation of HCHO.

According to Pei's study, a sorbent bed with higher than 80% breakthrough could be considered ineffective in practice for indoor air cleaning.⁴⁶ Hence, the 80% breakthrough point was chosen to

Table 1 Physical parameters of three nanocrystalline MnO₂.

Samples	Surface areas S_{BET} (m ² g ⁻¹)	Pore diameter D_p (nm)	Pore volume V_p (cm ³ g ⁻¹)
α -MnO ₂	70.11	14.48	0.13
γ -MnO ₂	74.84	15.70	0.24
δ -MnO ₂	87.50	19.85	0.28

identify the abilities of ACF and MnO₂/ACF in catalytic oxidation of HCHO. As shown in Fig. 5b, pure ACF had a fast breakthrough time of less than 60 min, and the 80% breakthrough time was nearly 100 min. In comparison, both of the breakthrough times of 0.01-MnO₂/ACF were prolonged to 50 min and 120 min, respectively. More MnO₂ contents could also lead to better catalytic activities, which could be proved by the results of 0.02-MnO₂/ACF and 0.03-MnO₂/ACF. However, when the MnO₂ content increased to more than 22.42% (critical point), the HCHO oxidation efficiency declined, suggesting that overload of MnO₂ might cause agglomeration of nanoparticles (see Fig. 2f), which blocked the pores of ACF substrates. Therefore, the optimal content of MnO₂ was set as 16.12%, in which, the 80% breakthrough time and formaldehyde removal capacities at 80% breakthrough point were 550 min and 0.74% (see Fig. S1).

The service life is a critical factor in practical applications for adsorbents and catalysts. The removal amount of HCHO by MnO₂/ACF at room temperature was tested (n=5) and the results are shown in Fig. 6. After 5 cycles, the removal capacity showed no significant difference when compared with the first cycle, while the yield of CO₂ presented a large variation. Besides, it's encouraging to see that the MnO₂/ACF could be reactivated by being dried at 130 °C for 4 h in vacuum. Based on the results of HCHO oxidation rate and CO₂ generation rate, the reactivated MnO₂/ACF was able to maintain its original function indicating HCHO molecules absorbed by active carbon fiber and MnO₂ could be partially degassed and removed by high temperature and vacuum pressure. The HCHO

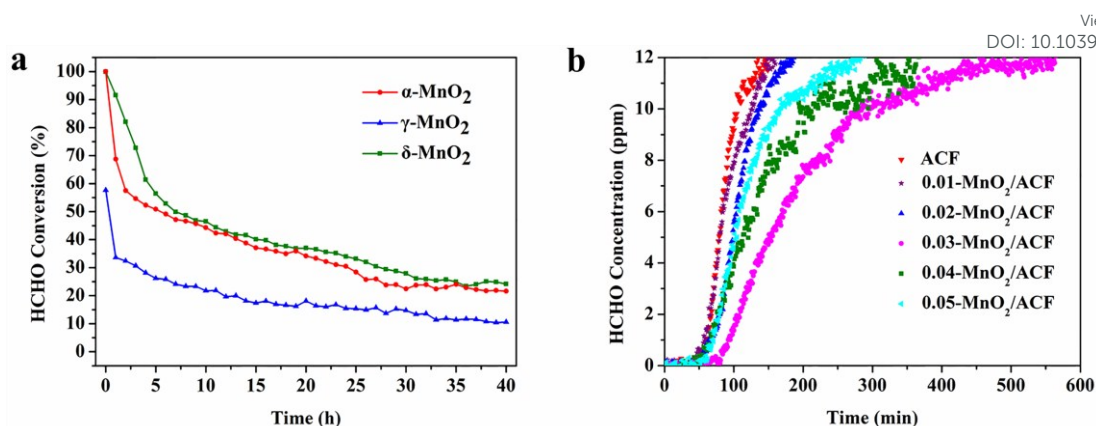


Fig. 5 (a) HCHO catalytic performance with time on stream over α -MnO₂, γ -MnO₂ and δ -MnO₂ catalysts. Reaction conditions: 25 °C, 15 ppm HCHO, 20 ± 2% RH, GHSV = 120 000 mL (gcat h)⁻¹. (b) Breakthrough curves of HCHO over ACF and MnO₂/ACF. Reaction conditions: 25 °C, 15 ppm HCHO, 20 ± 2% RH, GHSV = 60 000 mL (gcat h)⁻¹.

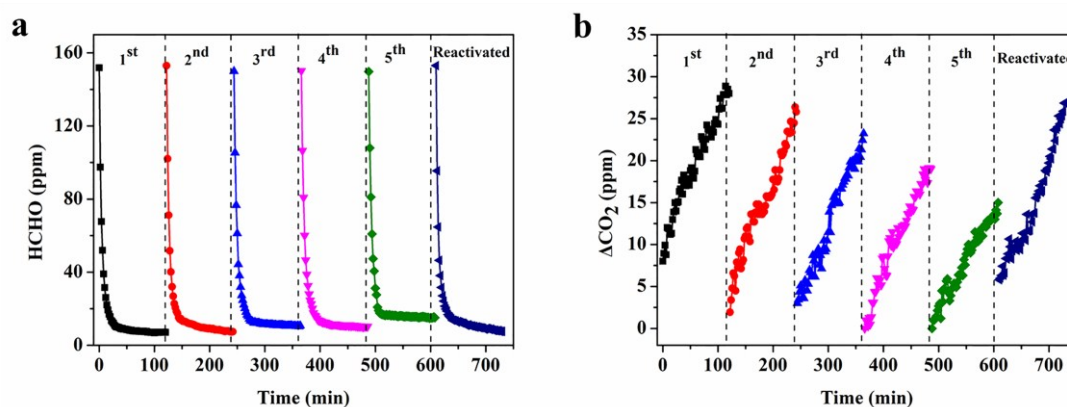


Fig. 6 Concentration variations of HCHO and CO₂ with reaction time for 0.03-MnO₂/ACF in the static recycle tests.

removal activity by MnO₂/ACF was a multiple process (see Fig. 8). Based on the previous reported results,^{13, 47-49} the mechanism of catalytic oxidation of HCHO with a catalyst was described as an adsorption-degradation-desorption process, which could also be used here to explain the oxidation process of HCHO using the MnO₂/ACF sample. As shown in Fig. 7, the concentration of HCHO decreased sharply in the first 60 min, after which the decreasing speed became slow. In comparison, the CO₂ concentration kept increasing linearly, regardless of the reaction time. Such trend indicated that the removal mechanism of HCHO could attribute to the absorption of ACF at the first 60 min and subsequent oxidation of MnO₂ till 540 min. Initially, most of the HCHO molecules were absorbed by active carbon and only a tiny proportion of HCHO was oxidized by MnO₂, emitting a small amount of CO₂. At the second stage, HCHO was oxidized by MnO₂ thus generating lots of CO₂.

Finally, the HCHO removal reached at a stationary state (stage III).

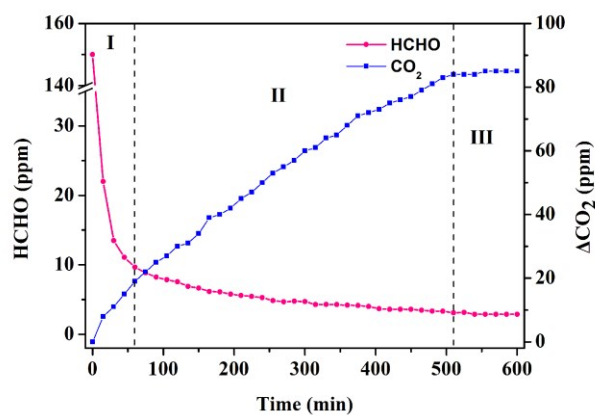


Fig. 7 Concentration variations of HCHO and CO₂ with reaction time for 0.03-MnO₂/ACF in the static test.

In general, the ACF substrate and nanocrystalline MnO_2 acted synergistically during the HCHO removal process. The MnO_2 provided catalytically active sites, and promoted the effective degradation of HCHO molecules. The ACF could provide fields for those active sites and also protect the MnO_2 from potential flue gas poisons. As compared with Table S1, the MnO_2 and MnO_2/ACF samples are competitive in HCHO oxidation at room temperature. Although the catalytic activity for HCHO oxidation of the MnO_2/ACF material is less effective than some noble metal catalysts, it has great advantage in catalytic HCHO removal at room temperature.

XPS Analysis. The surface electronic state of MnO_2/ACF was investigated by XPS analysis and the result was shown in Fig. 9 ("Before" represented the as-prepared sample while "After" represented the sample which had used in HCHO oxidation). After the deconvolution of Mn2p spectrum at $2p_{3/2}$, three peaks were emerged. The peaks at 642.6 eV and 641.5 eV indicated the presence of Mn^{4+} and Mn^{3+} , respectively, while another peak at 644.0 eV was assigned to satellite peak.⁵⁰⁻⁵² Compared with the spectra of as-prepared sample, the spectrum of after-test sample became broader and both peaks of Mn^{4+} and Mn^{3+} had a shift of 0.5 eV to a lower binding energy. This indicated that there was a significant change for the chemical state of manganese before and after reaction. MnO_2/ACF acted as catalysts in the oxidation process of HCHO. Table 2 further revealed the molar ratios of $\text{Mn}^{4+}/\text{Mn}^{3+}$ on the surface of as-prepared and after-test samples and the value decreased from 1.54 to 1.13. Zhang et al,⁶ recommended that more surface Mn^{4+} ions might provide more oxygen vacancies for an oxide material, which was positive to the adsorption, activation and migration of oxygen in the gas phase. For this reason, Mn^{4+} played an important role in HCHO oxidation and the redox cycle for

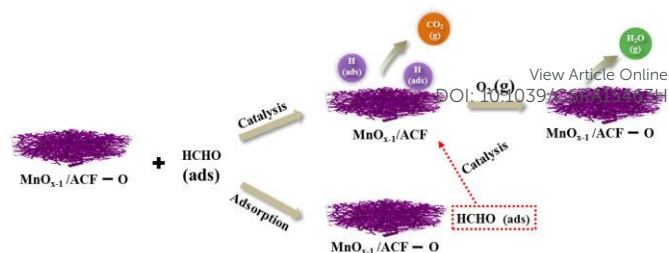


Fig. 8 The proposed mechanism for the catalytic oxidation of HCHO over MnO_2/ACF .

$\text{Mn}^{4+}/\text{Mn}^{3+}$ also occurred in the HCHO oxidation process. The deconvolution of O1s XPS spectra were displayed in Fig. 9b. The spectra of as-prepared sample were consisted of two main peaks at 530.0 and 531.4 eV. The former peak was attributed to the lattice oxygen (O^{2-}) denoted as O_{latt} , and the latter peak was assigned to surface adsorbed oxygen (such as OH) denoted as O_{ads} . From Table 2, it is clear that the surface molar ratios of $\text{O}_{\text{latt}}/\text{O}_{\text{ads}}$ of as-prepared and after-test samples were 1.71 and 0.55, respectively, suggesting that when the HCHO oxidation progress completed, the surface molar ratios of $\text{O}_{\text{latt}}/\text{O}_{\text{ads}}$ declined drastically. Another peak at a binding energy of 533.0 eV was caused by the presence of adsorbed water molecule on the surface of ACF and MnO_2 , which also appeared at the spectra of after-test sample. Room temperature oxidation of HCHO follows the Mars and van Krevelen mechanism as mentioned by previous studies, according to which the formaldehyde was finally oxidized to H_2O and CO_2 .⁴⁵ Therefore, it can be deduced that during the reaction, the formaldehyde was oxidized by the lattice oxygen of MnO_2 , and with the consumption of lattice oxygen, the molecular oxygen was generated in gas phase. These results proposed that abundant lattice oxygen would enhance the activity of MnO_2 catalysts for HCHO oxidation.

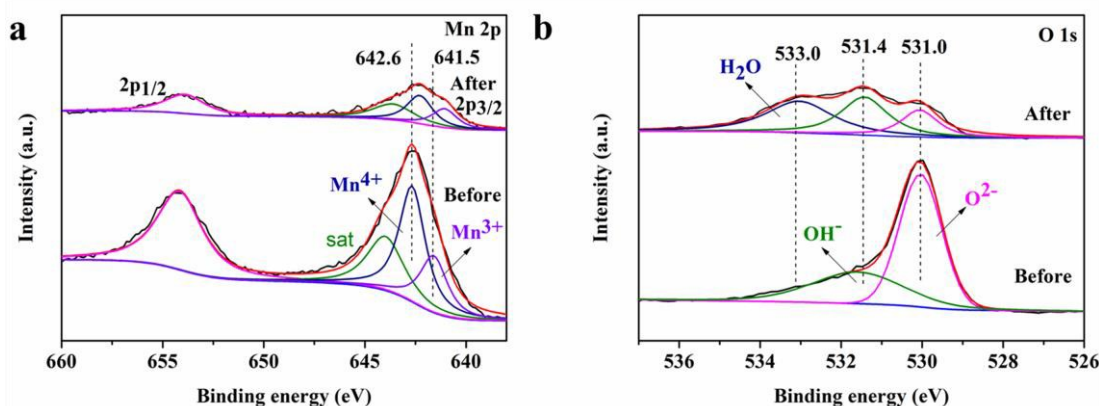
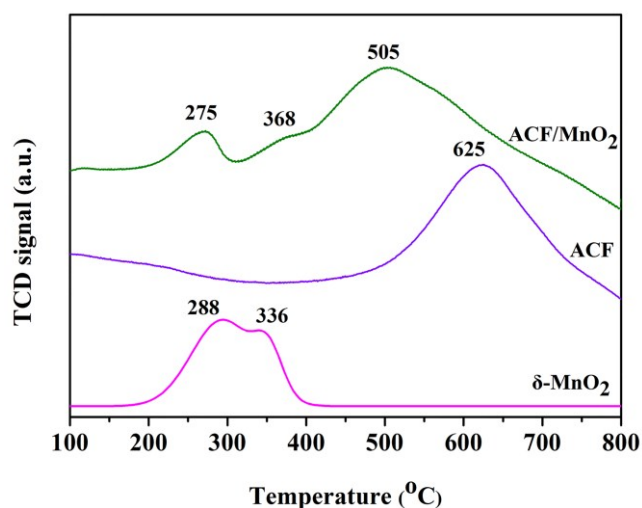


Fig. 9 XPS spectra of MnO_2/ACF samples: (a) Mn 2p and (b) O 1s.

Table 2 Physical parameters of three nanocrystalline MnO₂.View Article Online
DOI: 10.1039/C6RA15463H

Samples	Binding energy (eV)		Molecular ratio	Binding energy (eV)		Molecular ratio
	Mn ⁴⁺	Mn ³⁺	Mn ⁴⁺ /Mn ³⁺	O _{latt}	O _{ads}	O _{latt} /O _{ads}
As-prepared	624.6	641.5	1.54	531.0	531.4	1.71
After-test	642.1	641.0	1.13	531.0	531.6	0.55

Fig. 10 H₂-TPR profiles of the δ -MnO₂, ACF and MnO₂/ACF samples.

Reducibility of Catalyst. H₂-TPR measurements were performed to investigate the reducibility of the related samples. Fig. 10 showed the TPR profiles of δ -MnO₂, ACF and MnO₂/ACF. For the δ -MnO₂ catalyst, two reduction peaks were observed at 288 °C and 336 °C. It is obvious that the ratio of the lower temperature peak to the higher temperature peak was about 1, which could lead to the conclusion that the main product of the δ -MnO₂ catalyst could be MnO. The reduction route might be started with MnO₂ to Mn₂O₃, and then to MnO.^{6, 53} However, pure ACF displayed only one reduction peak of 625 °C, which should be attributed to the decomposition of functional groups, such as oxygenic groups in ACF sample. When nanocrystalline δ -MnO₂ were introduced into the ACF, the reduction behaviour was differed from that observed on the ACF. The TPR profiles of the MnO₂/ACF sample exhibited three reduction peaks, two of which shifted to lower temperature at 275 °C and 368 °C, while the other one shifted to 505 °C and showed higher peak intensity. The results illustrated that the decomposition of functional groups in the ACF was enhanced due to the existence

of nanocrystalline MnO₂.⁵⁴ In addition, since there existed an intense interaction between ACF and δ -MnO₂, MnO₂/ACF was more easily decomposed. To a certain extent, such decomposition could reflect the oxygen mobility in the samples. Since both δ -MnO₂ and ACF were involved with adequate mobile oxygen during the reaction, active oxygen would be motivated and enhanced the reduction of formaldehyde.

Conclusions

The α -MnO₂, γ -MnO₂ and δ -MnO₂ were successfully prepared by co-precipitation method. Formaldehyde catalytic oxidation results proved that all nanocrystalline MnO₂ had catalytic activities at room temperature, and the δ -MnO₂ obtained the highest activity. The influence of MnO₂ contents in MnO₂/ACF on the breakthrough time has also been studied and the optimal content of MnO₂ was found. The results suggest that the ACF substrate modified by nanocrystalline MnO₂ may be potentially used for formaldehyde removal in indoor environment.

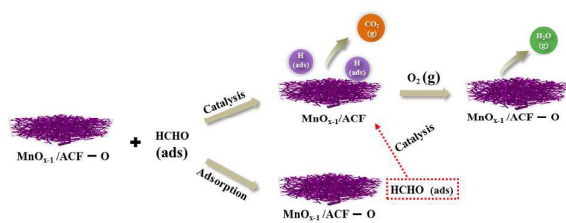
Acknowledgments

This work was supported by the Shanghai Municipal Science and Technology Commission (No. 14520502800), "Chen Guang" project supported by Shanghai Municipal Education Commission and Shanghai Education Development Foundation (NO. 14CG34) and Fundamental Research Funds for the Central Universities (NO. 2232014d3-15).

Notes and references

- V. J. Cogliano, Y. Grosse, R. A. Baan, K. Straif, M. B. Secretan and F. E. Ghissassi, *Environmental Health Perspectives*, 2005, **113**, 1205-1208.
- K. J. Lee, N. Shiratori, G. H. Lee, J. Miyawaki, I. Mochida, S.-H. Yoon and J. Jang, *Carbon*, 2010, **48**, 4248-4255.
- J. Pei and J. S. Zhang, *Hvac&R Research*, 2011, **17**, 476-503.
- D. Das, V. Gaur and N. Verma, *Carbon*, 2004, **42**, 2949-2962.

- 5 J. Peng and S. Wang, *Applied Catalysis B: Environmental*, 2007, **73**, 282-291.
- 6 J. Zhang, Y. Li, L. Wang, C. Zhang and H. He, *Catal. Sci. Technol.*, 2015, **5**, 2305-2313.
- 7 Y. Wan, X. Fan and T. Zhu, *Chemical Engineering Journal*, 2011, **171**, 314-319.
- 8 X. Zhu, X. Gao, R. Qin, Y. Zeng, R. Qu, C. Zheng and X. Tu, *Applied Catalysis B: Environmental*, 2015, **170-171**, 293-300.
- 9 H. M. Liu, X. J. Ye, Z. W. Lian, Y. G. Wen and W. F. Shangguan, *Research on Chemical Intermediates*, 2006, **32**, 9-16.
- 10 Y. Zhang, Y. Shen, X. Yang, S. Sheng, T. Wang, M. F. Adebajo and H. Zhu, *Journal of Molecular Catalysis a-Chemical*, 2010, **316**, 100-105.
- 11 Y. Shen, X. Yang, Y. Wang, Y. Zhang, H. Zhu, L. Gao and M. Jia, *Applied Catalysis B: Environmental*, 2008, **79**, 142-148.
- 12 X. F. Tang, J. L. Chen, Y. G. Li, Y. Li, Y. D. Xu and W. J. Shen, *Chemical Engineering Journal*, 2006, **118**, 119-125.
- 13 L. Zhou, J. He, J. Zhang, Z. He, Y. Hu, C. Zhang and H. He, *The Journal of Physical Chemistry C*, 2011, **115**, 16873-16878.
- 14 G. B. Baur, I. Yuranov and L. Kiwi-Minsker, *Catalysis Today*, 2015, **249**, 252-258.
- 15 J. H. Tsai, H. M. Chiang, G. Y. Huang and H. L. Chiang, *J Hazard Mater*, 2008, **154**, 1183-1191.
- 16 J. Economy, K. Foster, A. Andreopoulos and H. Jung, *Chemtech*, 1992, **22**, 597-603.
- 17 H. Rong, Z. Liu, Q. Wu, D. Pan and J. Zheng, *Cellulose*, 2009, **17**, 205-214.
- 18 Y.-C. Huang, C.-H. Luo, S. Yang, Y.-C. Lin and C.-Y. Chuang, *CLEAN - Soil, Air, Water*, 2010, **38**, 993-997.
- 19 D. Mo and D. Ye, *Surface and Coatings Technology*, 2009, **203**, 1154-1160.
- 20 L. Ma, D. Wang, J. Li, B. Bai, L. Fu and Y. Li, *Applied Catalysis B: Environmental*, 2014, **148-149**, 36-43.
- 21 Q. Xu, W. Lei, X. Li, X. Qi, J. Yu, G. Liu, J. Wang and P. Zhang, *Environ Sci Technol*, 2014, **48**, 9702-9708.
- 22 X. Tang, Y. Li, X. Huang, Y. Xu, H. Zhu, J. Wang and W. Shen, *Applied Catalysis B: Environmental*, 2006, **62**, 265-273.
- 23 B. Bai, H. Arandiyani and J. Li, *Applied Catalysis B: Environmental*, 2013, **142-143**, 677-683.
- 24 S. Bai, H. Liu, J. Sun, Y. Tian, R. Luo, D. Li and A. Chen, *RSC Adv.*, 2015, **5**, 48619-48625.
- 25 J. Y. Kim, N.-J. Choi, H. J. Park, J. Kim, D.-S. Lee and H. Song, *The Journal of Physical Chemistry C*, 2014, **118**, 25994-26002.
- 26 X. Yu, J. He, D. Wang, Y. Hu, H. Tian, T. Dong and Z. He, *Journal of Nanoparticle Research*, 2012, **14**.
- 27 X. Yu, J. He, D. Wang, Y. Hu, H. Tian and Z. He, *The Journal of Physical Chemistry C*, 2012, **116**, 851-860.
- 28 L. Zhou, J. Zhang, J. He, Y. Hu and H. Tian, *Materials Research Bulletin*, 2011, **46**, 1714-1722.
- 29 L. Qi, B. Cheng, J. Yu and W. Ho, *Journal of Hazardous Materials*, 2016, **301**, 522-530.
- 30 Y. C. Huang, B. Long, M. N. Tang, Z. B. Rui, M. S. Balogun, Y. X. Tong and H. B. Ji, *Applied Catalysis B-Environmental*, 2016, **181**, 779-787.
- 31 L. Nie, Y. Zheng and J. Yu, *Dalton Trans*, 2014, **43**, 12935-12942.
- 32 X. H. Yu, J. H. He, D. H. Wang, Y. C. Hu, H. Tian, T. X. Dong and Z. C. He, *Journal of Nanoparticle Research*, 2013, **15**.
- 33 C. B. Zhang, H. He and K. Tanaka, *Catalysis Communications*, 2005, **6**, 211-214.
- 34 J. Q. Torres, S. Royer, J. P. Bellat, J. M. Giraudon and J. F. Lamonier, *Chemsuschem*, 2013, **6**, 578-592.
- 35 L. H. Nie, J. G. Yu, M. Jaroniec and F. F. Tao, *Catalysis Science & Technology*, 2016, **6**, 3649-3669.
- 36 Y. Sekine, *Atmospheric Environment*, 2002, **36**, 5543-5547.
- 37 I. Roche and K. Scott, *Journal of Electroanalytical Chemistry*, 2010, **638**, 280-286.
- 38 J. Yang, L. Zou, H. Song and Z. Hao, *Desalination*, 2011, **276**, 199-206.
- 39 G.-Y. Oh, Y.-W. Ju, H.-R. Jung and W.-J. Lee, *Journal of Analytical and Applied Pyrolysis*, 2008, **81**, 211-217.
- 40 M. El-Merraoui, M. Aoshima and K. Kaneko, *Langmuir*, 2000, **16**, 4300-4304.
- 41 L. Peng, Y. Chen, H. Dong, Q. Zeng, H. Song, L. Chai and J.-d. Gu, *Water, Air, & Soil Pollution*, 2015, **226**.
- 42 M. Wang, H. Liu, Z.-H. Huang and F. Kang, *Chemical Engineering Journal*, 2014, **256**, 101-106.
- 43 K. S. W. Sing, D. H. Everett, R. A. W. Haul, L. Moscou, R. A. Pierotti, J. Rouquerol and T. Siemieniewska, *Pure and Applied Chemistry*, 1985, **57**, 603-619.
- 44 T. Chen, H. Dou, X. Li, X. Tang, J. Li and J. Hao, *Microporous and Mesoporous Materials*, 2009, **122**, 270-274.
- 45 S. Devaraj and N. Munichandraiah, *Journal of Physical Chemistry C*, 2008, **112**, 4406-4417.
- 46 J. Pei and J. S. Zhang, *Chemical Engineering Journal*, 2011, **167**, 59-66.
- 47 C. Cellier, V. Ruau, C. Lahousse, P. Grange and E. M. Gaigneaux, *Catalysis Today*, 2006, **117**, 350-355.
- 48 C. Doornkamp and V. Ponec, *Journal of Molecular Catalysis a-Chemical*, 2000, **162**, 19-32.
- 49 M. A. Sidheswaran, H. Destailats, D. P. Sullivan, J. Larsen and W. J. Fisk, *Applied Catalysis B-Environmental*, 2011, **107**, 34-41.
- 50 B. Bai, J. Li and J. Hao, *Applied Catalysis B-Environmental*, 2015, **164**, 241-250.
- 51 P. Mahamallik, S. Saha and A. Pal, *Chemical Engineering Journal*, 2015, **276**, 155-165.
- 52 S. Ponce, M. A. Pena and J. L. G. Fierro, *Applied Catalysis B-Environmental*, 2000, **24**, 193-205.
- 53 S. Liang, F. T. G. Bulgan, R. Zong and Y. Zhu, *Journal of Physical Chemistry C*, 2008, **112**, 5307-5315.
- 54 S. R. de Miguel, J. I. Villella, E. L. Jablonski, O. A. Scelza, C. S. M. de Lecea and A. Linares-Solano, *Applied Catalysis a-General*, 2002, **232**, 237-246.



A synergistic catalytic removal of HCHO was achieved over Nanocrystalline MnO₂ modified activated carbon fiber at room temperature.